PLANAR AND NON-PLANAR PRINT PATTERNS IN PEEK FLAT BACKUP RINGS TO INCREASE SEAL PERFORMANCE UNDER HIGH PRESSURE AND TEMPERATURE

J. T. Green*, I. A. Rybak*, J. W. McKee†, and C. Glaesman‡

*Department of Engineering Education and Leadership, The University of Texas at El Paso, El Paso, TX 79968

†Department of Aerospace and Mechanical Engineering, The University of Texas at El Paso, El Paso, TX 79968

‡Halliburton Energy Services, Singapore

Abstract

Numerous industries use thermoplastics to meet the demanding requirements of high-temperature and high-pressure sealing applications. Flat backup rings, common components of sealing assemblies, can be additively manufactured using fused filament fabrication and can perform comparably to their conventionally manufactured counterparts. The load response which develops within the seals is largely driven by pressure and the geometry of the extrusion gap which is located opposite of the primary seal in the assembly. To better address this loading condition, flat backup rings were fabricated with conventional print patterns and compared to custom radial print patterns which were configured with planar and non-planar layer configurations. Specimens underwent pressure vessel tests to provide an estimate of seal performance at high-pressure and high-temperature. The observed relationship between test results and print orientation may inform tuning of sealing structures in numerous industries to further optimize seals for multiple objectives.

Keywords: Non-planar Printing, Sealing Assembly, Fused Filament Fabrication, PEEK, Backup Ring, Oil and Gas

Introduction

Injection molding is among the most common conventional thermoplastic manufacturing processes in industry [1]. Additive manufacturing (AM) with thermoplastics often fails to achieve competitive properties, such as density and tensile strength, when compared to their injection molded counterparts [2]. For mechanical applications, this is often a function of the anisotropy observed in AM thermoplastics relative to the loading conditions of the application [3,4]. Notably, creep is a mechanism of deformation for which AM thermoplastics may achieve comparable performance relative to their injection molded counterparts for some load orientations depending on the design and implementation of the AM process [5,6]. Creep performance is a critical indicator for seal assembly performance indicating the potential for AM to produce seals having extraordinary performance [7].

Freedom of design in AM far exceeds that of conventional manufacturing processes. Complex geometries can be produced by these manufacturing techniques including advanced

features like internal voids [8,9] and lattice structures [10]. Numerous parameters can be finely tuned in AM processes to alter the material's structure and properties [11]. Some methods like fused filament fabrication (FFF) can further control such material features as fiber orientation by tailoring toolpaths during printing [12]. Adding to the complexity of these parameters is non-planar, also known as conformal, printing which enables toolpaths to traverse all three spatial dimensions [13]. Tuning of these features has been investigated for the benefit of numerous applications [14]. As much as this design freedom provides opportunities to improve print results, it poses a challenge to the designer who must parse through the many combinations of print parameters and toolpaths to yield the desired geometry and properties [15]. The extreme complexity of these manufacturing techniques continues to necessitate experimental studies.

Recently, design freedom in AM significantly increased due to technological advancements enabling local composition control (LCC) [16–19]. In addition to the other features and parameters described previously, now the composition within the printed structures can be varied throughout their volume. An active-mixing hotend has been paired with an FFF printer to enable controlled mixing of multiple filaments including control of fiber volume fractions [20]. With this wide variety of possibilities has led to research into tailoring the AM parts for specific applications and load conditions. Due to their dependence on creep performance, sealing systems have been investigated as a potential application for thermoplastic AM.

Results were presented at the International Petroleum Technology Conference by Green et al. which achieved comparable performance to injection molded flat backup rings (FBUR) through AM as demonstrated using Poly Ether Ether Ketone (PEEK) and PEEK reinforced with carbon fiber (PEEK+CF) [21]. Green et al. explored the effects of distributing carbon fiber (CF) in different regions of the FBUR and evaluated the performance of the corresponding sealing assemblies through pressure vessel tests (Figure 1). An all-metal hotend was used in an FFF printer when printing PEEK FBUR's with filaments assigned by layer to either form uniform FBURs or FBURs having two distinct regions, one region composed of PEEK and the other composed of PEEK+CF. To better understand the effects of varying fiber volume fractions (FVF) throughout the structure, an active-mixing hotend was used to dynamically vary filament mix ratios of Polylactic acid (PLA) and PLA reinforced with CF (PLA+CF). Polylactic acid was used instead of PEEK due to the temperature limits of the active-mixing hotend used in that study. In both cases, the distribution of CF greatly impacted seal assembly performance pressure vessel tests to measure creep deformation and extrusion to failure. All of these specimens were printed following a custom pattern including radially oriented infill, but the study did not assess the impact of using this pattern. This study by Green et al. indicates the potential for FFF to expand the performance of FBURs without modifying size or average composition.

This study seeks to further expand capabilities for FBUR AM and to better understand the impact of toolpaths on PEEK printing. By printing PEEK FBURs using a high-temperature active-mixing hotend, a major advancement towards LCC can be demonstrated indicating support for future work investigating composite architectures in PEEK FBURs. With high-temperature thermoplastic printing demonstrated, an increased understanding of FBUR printing can be determined by varying print patterns to increase our understanding of how print orientation affects FBUR performance. The specific objectives of this study include the following:

1. Develop an active-mixing hotend that can operate at 400 °C to facilitate printing with PEEK and configure it to operate with an FFF printer.
2. Enable non-planar printing in the FFF printer facilitated by tilting the print bed.
3. Print FBURs with planar concentric, rectilinear, and radial infill patterns and evaluate performance through pressure vessel tests.
4. Print FBURs with non-planar radial infill patterns with positive 5° tilt (conical +5°) and negative 5° tilt (conical -5°) with performance evaluated through pressure vessel tests.

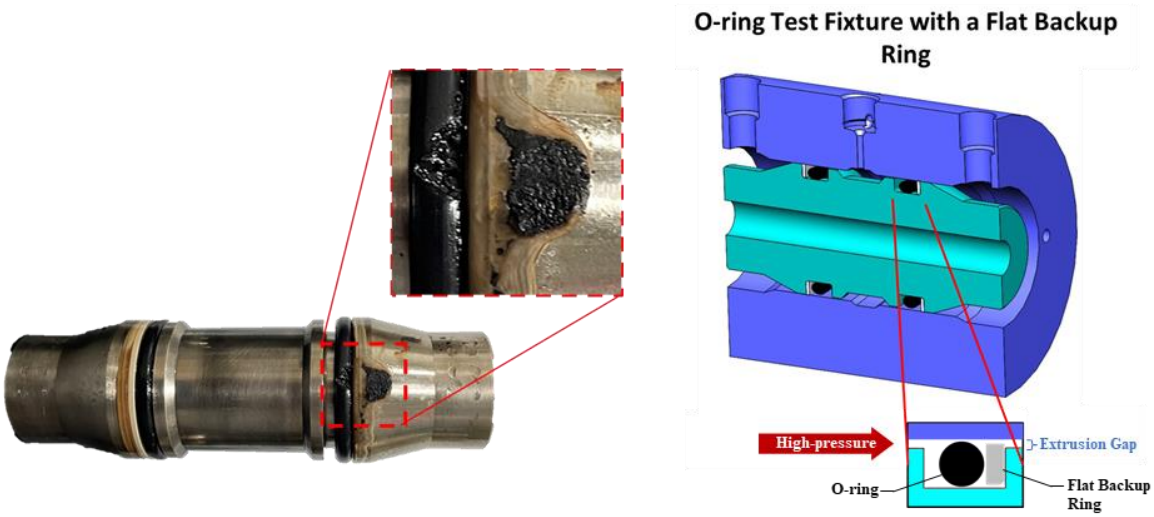

Figure 1 – Sealing assembly image and diagram. Diagram depicts the cross section of an O-ring test fixture with a flat backup ring. Left image illustrates failure of a primary seal and flat backup ring after a test following an extrusion-to-failure test protocol. Damage to the primary seal is visible as is residue from the primary seal located on the damaged flat backup ring. Material from both the flat backup ring and the primary seal have been deposited or deformed into the extrusion gap located between the mandrel and test fixture.

Methods

High-temperature mixing printer development

The mixing printer previously used to investigate variable FVFs in FBURs included an active-mixing hotend with a spring-energized, polymeric seal in contact with the mixing rod to prevent leaking from the heated mixing chamber. This seal's 230 °C operational limit prevented hotend compatibility with materials like PEEK, which has a recommended hotend temperature of approximately 400 °C. To facilitate this increase in temperature limits, a new active-mixing hotend was designed. A graphite seal was included in the design which is rated to operate at or above the 400 °C setpoint required for PEEK printing. This seal does not energize itself and requires external force to be applied to it. This requirement was met by using springs which press the seal against the hotend above the heated chamber. This hotend was paired with DyzeXtruder Pro extruders (Dyze Design, LeMoyne, Quebec, Canada) and modified Mosquito® Liquid heatbreak assemblies (Slice Engineering, Gainesville, FL, USA) at each inlet.

The new extruder assembly including the high-temperature mixing hotend was mounted on a carriage which is positioned through use of a custom parallel gantry system actuated by belt driven stepper motors to control motion along the printer's X-axis and Y-axis. A bed sensor was

mounted on the carriage to assist with bed levelling and homing the Z-axis. The print bed is a Funmat HT heated bed (Intamsys Technology Co. Ltd., Shanghai, China) and was actuated by three separate lead screws connected to the bed carriage through magnetic ball joints and driven by stepper motors. The bed configuration having three parallel actuators controlling bed motion facilitates bed tilt for operations like automated tramming of the bed surface. The controller board was a Bigtreetech Octopus Pro V1.1 with the Bigtreetech Motor Expansion Board (Shenzhen Big Tree Technology Co. Ltd., Shenzhen, China), flashed with Marlin 2.1.x firmware (marlinfw.org) [22] configured for the custom printer gantry, active-mixing, and high temperature printing. Each motor is controlled by a Trinamic TMC2209 stepper driver (Analog Devices Inc., Wilmington, MA, USA) to enable precise positional control and synchronous motion. Solid-state relays were incorporated into the control system to offload the high current bed and extruder heaters from the control board. This design supports printing with PEEK filaments and provides a rigid structure by which this heavy hotend can be accurately positioned. An image of the computer model of the high-temperature mixing printer with the new hotend is presented in Figure 2.

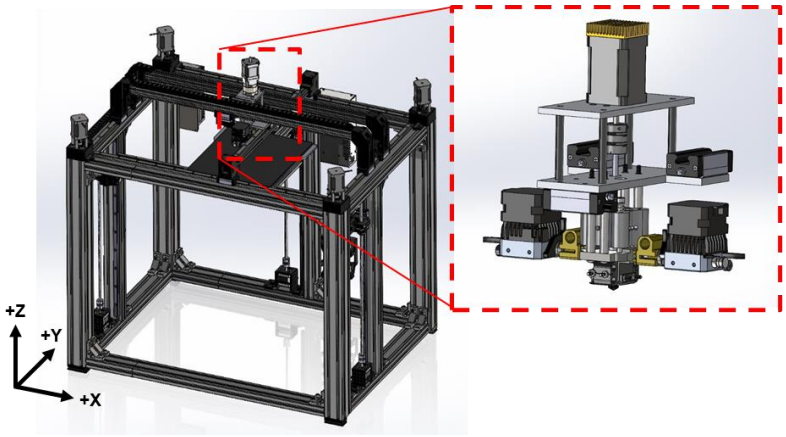

Figure 2 - Computer model of the high temperature mixing printer with a custom high- temperature, active-mixing hotend. Four stepper motors are positioned on the top of the printer to drive motion in the X and Y directions through a parallel gantry configuration. The print bed position is controlled by three stepper motors positioned at the bottom of the printer for which each turn a lead screw connected to the print bed's carriage. The detail image shows the high temperature hotend connected to its corresponding carriage. The top motor controls the mixing rod which is held in place by a bearing housing. Each filament inlet is connected to a water-cooled heat break and a corresponding extruder. The nozzle at the bottom of the printer is threaded enabling nozzle replacement and adjustment of nozzle diameter.

Flat backup ring geometry, general print configuration, and post-processing

A simple FBUR geometry was used in this work matching the geometry which was used in a previous study [21]. All specimens were printed with 1.75 mm diameter PEEK filament (Essentium Inc., Pflugerville, TX) on the new high-temperature mixing printer in open air with mixing rod rotation set to 17.46 revolutions per mm of filament extruded. The filament was dehydrated for a minimum of 24 hours in an oven set to 100 °C and stored in a dry box during printing. The side of the FBUR which contacts the O-ring, the primary seal of the assembly, was printed face down to ensure a smooth surface which would not compromise the integrity of the O-ring. The digital thread for planning print operations to produce FBURs is presented in Figure 3, and the corresponding print parameters are provided in Table 1. Specimens were tuned iteratively by adjusting print parameters and optically evaluating FBUR cross sections. The scarf cuts were formed during printing but were lightly bonded shut due to the overhang in the configuration. After printing, specimens were post-processed in preparation for pressure vessel testing. The brims were

removed, and the scarf cut was prepared by cutting it open and lightly sanding the surfaces to ensure smooth articulation during FBUR operation.

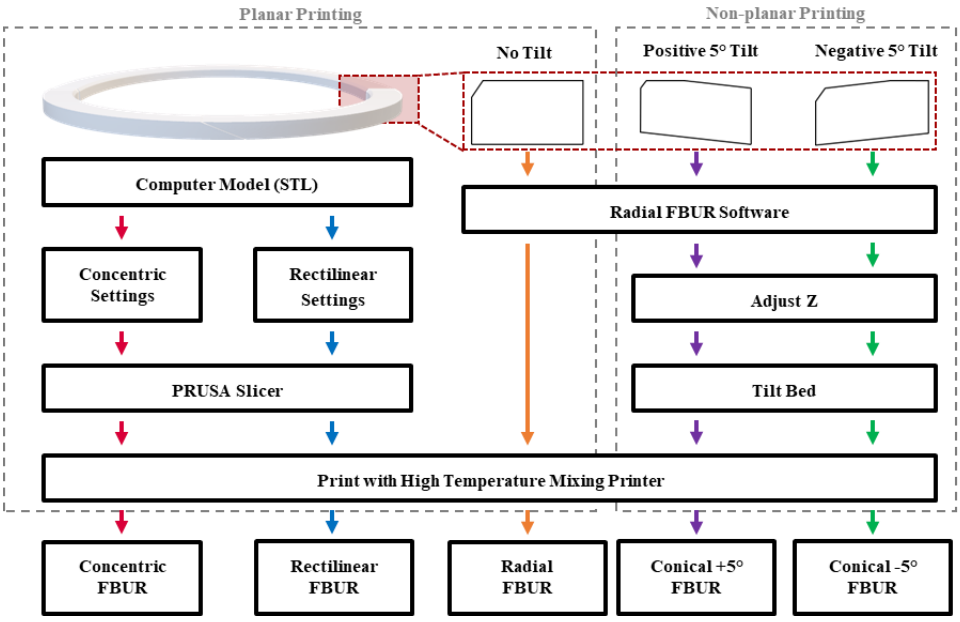

Figure 3 - Diagrams depicting print patterns produced using the custom flat backup ring software. Infill patterns are oriented radially with extrusion width varied to prevent gaps between toolpaths. Variations in extrusion width are facilitated by changing print speed such that the volumetric flow rate through the hotend remains constant. Each layer is offset by half of an extrusion width which generates an offset brick-pattern reducing voids between extrusions by positioning the toolpaths of a new layer between the previous layer's toolpaths.

Table 1 - Print settings for each type of flat backup ring

Identifier for FBUR Type	G-code Slicer	Additional Processing	Extrusion Multiplier	Max Extrusion Width/Height (mm)	Max Speed Print/Travel (mm/s)	Perimeter Width (mm)	Layers	Bed Material	Perimeter Infill Overlap (%)
Concentric	Prusa[1]	-	1.02	0.90/0.20	15/100	0.4	9	Carbon Fiber	35
Rectilinear	Prusa[1]	-	1.02	0.90/0.20	15/100	0.4	9	Carbon Fiber	30
Radial	Custom FBUR Software	-	0.95	0.90/0.20	20/100	0.4	9	Carbon Fiber	10
Conical +5°	Custom FBUR Software	N-P	0.92	0.60/0.20	20/100	0.6	10[2]	Glass	40
Conical -5°	Custom FBUR Software	N-P	0.92	0.60/0.20	20/100	0.6	10[2]	Glass	40

N-P: non-planar G-code modifications including Z-coordinate adjustments, code for bed tilting, XYX-coordinate tracking during bed tilting

Notes:
1) PrusaSlicer 2.7.2 (Prusa Research s.r.o., Prague, Czech Republic).
2) Layer height and size is altered when converted to conical layers.

Planar flat backup ring fabrication

Rectilinear and concentric FBUR print files were prepared using PrusaSlicer 2.7.2 (Prusa Research s.r.o., Prague, Czech Republic). The radial infill was prepared using custom FBUR software with an unmodified profile corresponding with the desired FBUR geometry (Figure 4). The planar FBUR specimens were printed on a CF print bed which experienced progressive damage on its top surface, a common problem when printing with PEEK. Print previews of the planar FBUR prints are provided in Figure 5. These planar FBURs were fabricated without the printer modifications described in the section below. Eight specimens of each FBUR configuration were printed. Six specimens of each type were used for pressure vessel testing, three for extrusion to failure tests and three for creep tests. As for the other two specimens, one was cross-sectioned and optically analyzed while the other was used for density measurements.

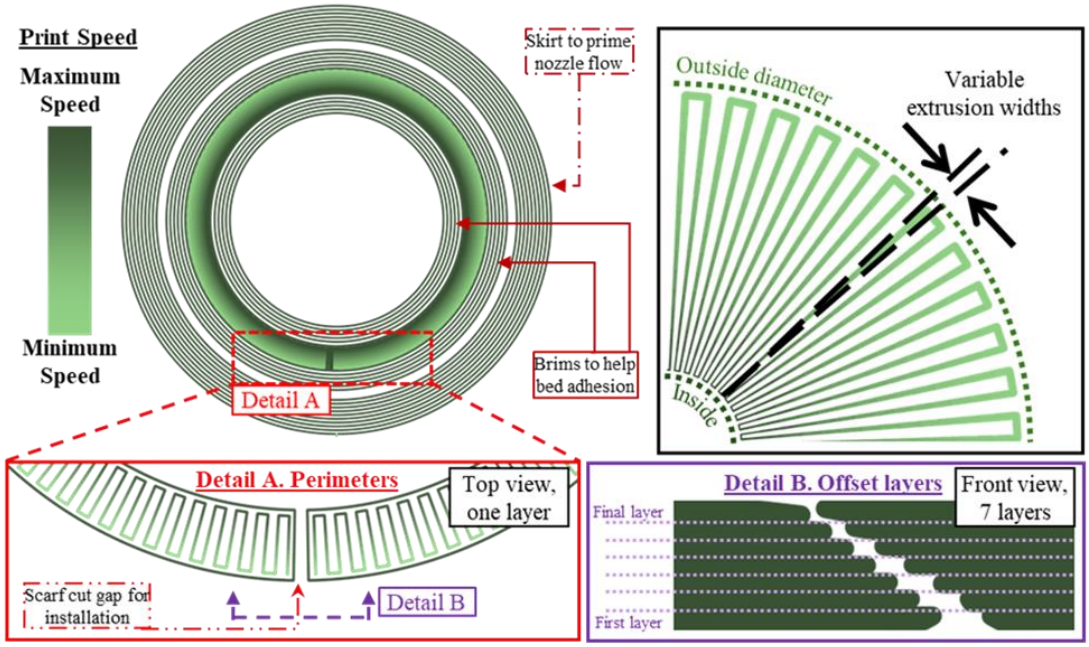

Figure 4 - Diagrams depicting print patterns produced using the custom flat backup ring software. Infill patterns are oriented radially with extrusion width varied to prevent gaps between toolpaths. Variations in extrusion width are facilitated by changing print speed such that the volumetric flow rate through the hotend remains constant. Each layer is offset by half of an extrusion width which generates an offset brick-pattern reducing voids between extrusions by positioning the toolpaths of a new layer between the previous layer's toolpaths.

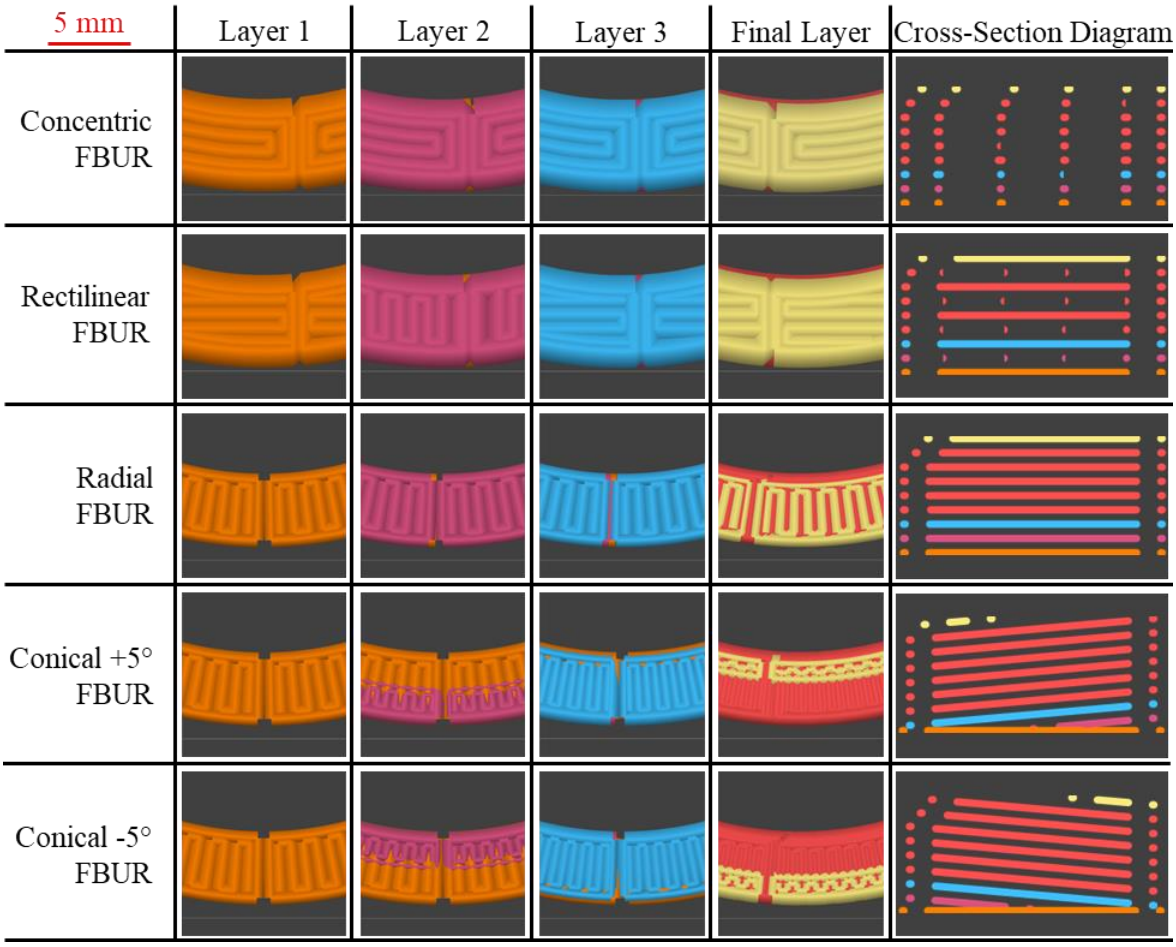

Figure 5 - Print previews for the five print patterns and corresponding diagrams of their cross-sections. Print previews are viewed from above at the scarf cut and include within the image all layers from the print bed up to the layer indicated by the label in the top row. The cross-section diagrams indicate the centerline of the toolpaths in and out of page using circles and indicate toolpaths that are parallel to the page using lines. Colors are modified on a layer-by-layer basis to provide contrast and coordination across columns.

Mixing printer modifications and homing operations for non-planar printing

The Marlin 2.1.x firmware system does not support dynamic bed tilt during printing, only individual actuator motion for leveling. To enable tilt during printing, the firmware was modified to provide individual control of each bed actuator during print processes rather than treat them as a system of actuators which collectively provide a single axis of control. These actuators were assigned labels Z, V, and W. The printer was flashed with a modified version of Marlin firmware based on bugfix-2.1.x, distribution date June 15, 2024. In addition to configuring additional axes identified as V and W in print commands, the firmware modifications allow for the synchronization of these axes with the primary Z axis, now configured as a single motor, during homing and calibration procedures. When homing any of the three axes, all three simultaneously move up and down to maintain the level plane of the bed relative to the sensor. Print commands were formatted as "G1 X# Y# Z# V# W# F#" where Z V W correspond with the position of the three vertical motors, including negative axis space which is sometimes necessary for axes to reach

necessary tilt levels of the bed. Each of these three motors is homed using the bed sensor by probing a point on the bed near the corresponding ball joint. This operation is performed sequentially for each motor, a combination of operations which is then repeated ten times to ensure precise homing results.

The mixing printer design as originally developed for this study mechanically supports bed tilt but has numerous conflict points limiting the range of tilt to approximately 1° when printing near the surface of the print bed. Since the ball joints connected to the print bed were located far from the center of the bed, a large range of vertical motion was necessary per increment of bed tilt. To increase the range of tilt without collision, the bed carriages were redesigned to position the ball joints nearer to the print bed. This change increased the range of tilt with the new limits to rotation being collision with the bed sensor and the extruder assembly itself. A custom mount was designed and integrated into the printer making the bed sensor removeable enabling 10° of bed tilt in all directions. The physical changes to the printer and the limiting conflict point are visible in Figure 6.

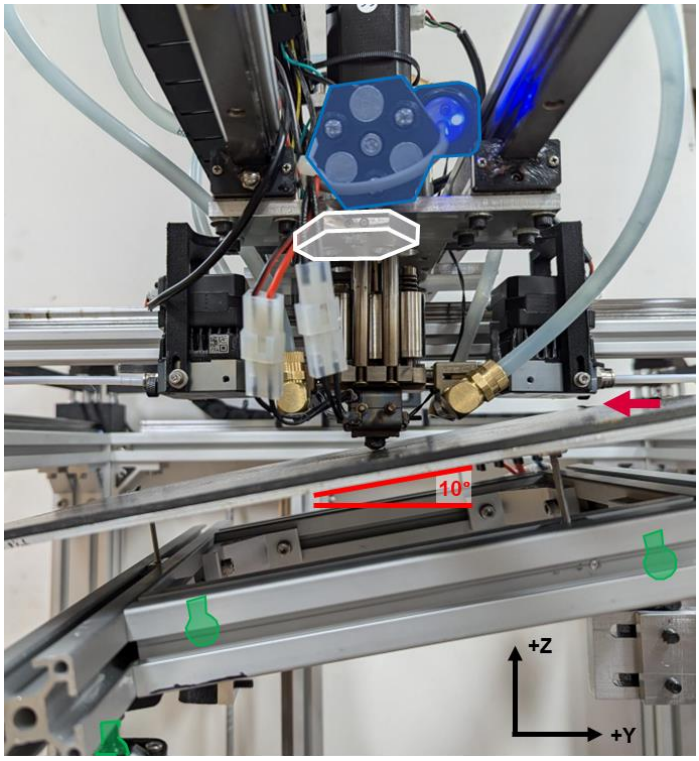

Figure 6 - Image of the mixing printer with the bed rotated about the printer's X-axis with tilt set to 10°. The red arrow indicates the conflict point where the extruder on the right would collide with the bed if the print bed was tilted further. The green icons indicate the modified location of the ball joints which enables increased bed tilt. The white icon indicates the mounting apparatus where the removable bed sensor, as is indicated in blue, is mounted during probing operations.

Non-planar digital thread and supporting software

A digital thread containing custom processes and software was developed for planning non-planar print operations using the mixing printer as configured for bed tilt. In this approach, the Z-component of the desired geometry is shifted in proportion to the desired angle for slicing. The geometry is then sliced in a traditional layer-by-layer fashion before it is processed by custom

software to adjust the Z-component of the print commands such that the print commands follow the desired non-planar tool paths. The extrusion volumes of print moves were scaled as a proportion of the effective Z-adjusted layer thickness relative to the layer thickness as assigned in the slicing software. At this phase of processing, the printer can follow these instructions and may yield a print resembling the intended structure, but bed tilt would not be implemented effectively leaving the deposition angle unadjusted which may cause poor print quality due to effects like the nozzle scraping the print during printing. In the final phase of print planning, commands were adjusted to facilitate bed tilt including motion to move the nozzle so that it tracks with the intended location relative to the print bed. Motion to facilitate bed tilt is determined in this software using the equation for a plane and vector rotation. These calculations assume that the ball joints connected to the print bed do not change in their X and Y locations. This assumption is more inaccurate at high tilt angles and is only reasonable for prints with low tilt angles. To promote adhesion to the print bed, a flat first layer using a radial print pattern was added to the print file shifting the conical prints up one layer thickness. Note that the profile of the non-planar prints was reduced in thickness to yield an accurate geometry after adding the flat first layer. When removing the brim, a razor was used to ensure that the flat first layer aligned well with the nonplanar region of the print. An example of this process applied to a rectangular prism (.stl) with a constant bed tilt and conventional slicing is presented in Figure 7.

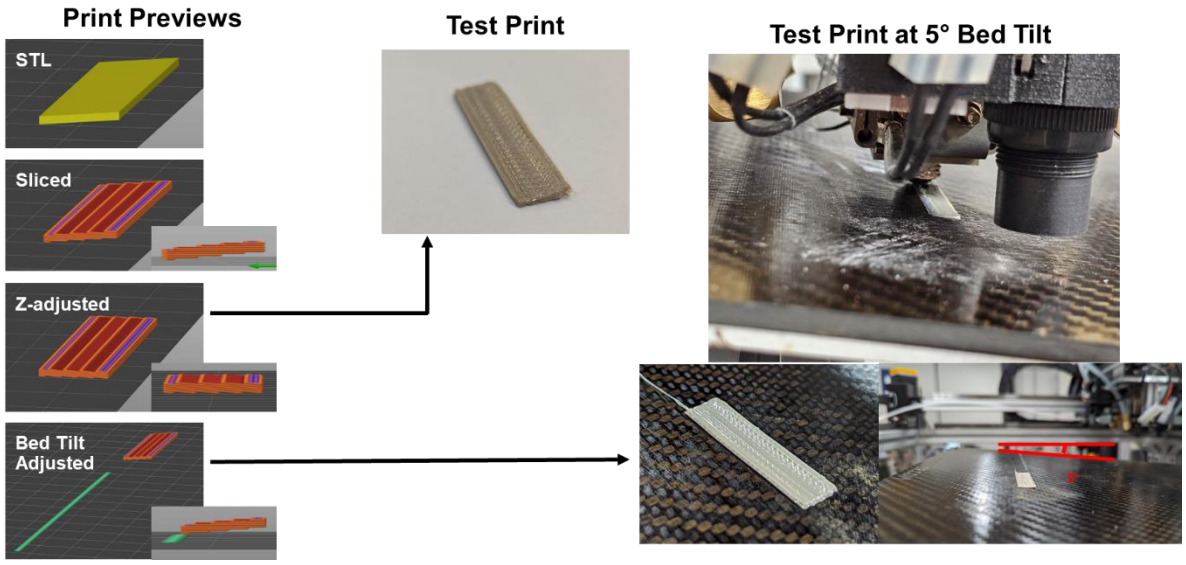

Figure 7 – Example of print process for non-planar printing including print previews and images of test prints with and without bed tilt.

Non-planar flat backup ring fabrication

Non-planar FBURs were printed with the bed tilted in two configurations, inward and outward relative to the center of the FBUR to form conical layers. Software was developed which prepares input commands for the profile used in the custom FBUR software. This profile includes changes in the Z-components of the profile according to the desired tilt and is presented in Figure 3 for both configurations. The output from the FBUR software was then processed following the digital thread previously described for non-planar printing. These specimens were printed with 5° tilt angles since large tilt angles resulted in print errors due to ball joint translation as is visible in

Figure 8. The FBURs which were printed with the layers tilted inward are labelled “conical +5°” while the FBURs with layers tilted outward are labelled “conical -5°.” Eight specimens of each FBUR configuration were fabricated. Six specimens of each type were used for pressure vessel testing, three for extrusion to failure tests and three for creep tests. As for the other two specimens, one was cross-sectioned and optically analyzed while the other was used for density measurements.

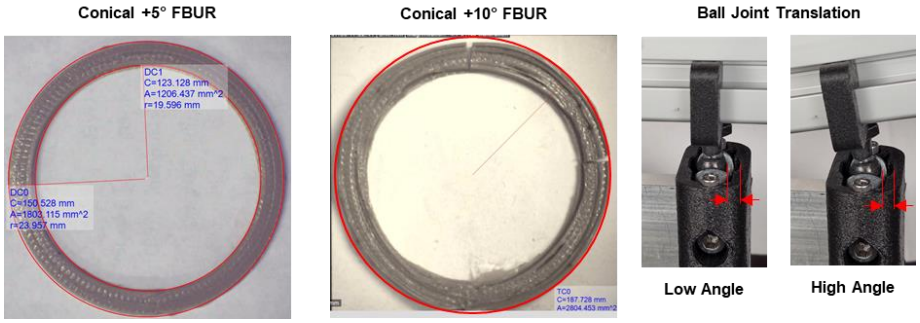

Figure 8 – Demonstration of non-planar printing at high and low tilt angles. At large angles, ball joints translate inconsistently resulting in geometric inaccuracies which can be seen as a lack of roundness in the conical 10° FBUR.

Pressure Vessel Test Procedures

Sealing systems commonly use PEEK FBURs which are traditionally manufactured through injection and compression molding methods. Pressure vessel test parameters were selected to be identical to the tests in the previous study which investigated the impact of composite architectures on FBUR performance. The use of these parameters ensures that these tests are comparable to conventionally manufactured FBURs and the PEEK FBURs of the previous study. The fixture was configured for testing ISO3601-1 sized -325 O-rings (inside diameter = 34.47 mm and diameter of the cross section = 5.33 mm). The extrusion gap in this configuration is 0.305 mm. In each test, the test FBUR was paired with an O-ring having a durometer hardness of 90A (Figure 1). Two sets of pressure vessel tests were performed. Extrusion to failure tests held the temperature of the vessel at a constant 260 °C and ramped up pressure in increments of 13.8 MPa until the seal assembly ruptured. The output for this test is the pressure at rupture. Creep tests are performed by holding the pressure vessel temperature at a constant 232 °C and a constant pressure of 124.1 MPa for 120 hours. The thickness of the FBUR is measured in four locations before testing and measured again after testing. The average difference in measurements is the output from this test.

Density measurement and void characterization

Density measurements were performed using the Archimedes’ principle. The specimen was weighed in air and then weighed again while submerged in water. The difference in weight was used to determine the volume of water which was displaced by the specimen. The density was then calculated using the weight in air and dividing it by the calculated volume of water which was displaced. Void content was calculated by comparing the difference in the measurement relative to the expected density of PEEK which is 1.32 g/cm^3.

Results

Printed flat backup rings and printer demonstration

All five types of PEEK FBURs were successfully printed demonstrating effective print planning operations and success in developing the high-temperature mixing printer. Although only one filament was used in printing, it was printed at a hotend temperature setpoint of 400 °C and paired with mixing rod rotation indicating the functionality which enabled LCC and FVF control in previous work [21]. Accuracy in printing FBURs following the variety of print patterns is evident in the cross-sections presented in
Figure **9**. The concentric print pattern when using these print settings yields the most accurate cross-section geometry and the smoothest surfaces as compared to the other print patterns. The concentric print pattern contains large travel moves which leave behind large gaps within the print but were not observable in the cross sections since the cross sections do not intersect the locations where the defects are present. The petal print pattern has the fewest voids visible in the cross sections indicating that the brick-pattern formed by shifting layers half an extrusion width and tuning print speeds to control extrusion width are effective techniques for densely packing the FBUR print volume. The non-planar print angles indicating conical layers are visible in the radial cross sections.

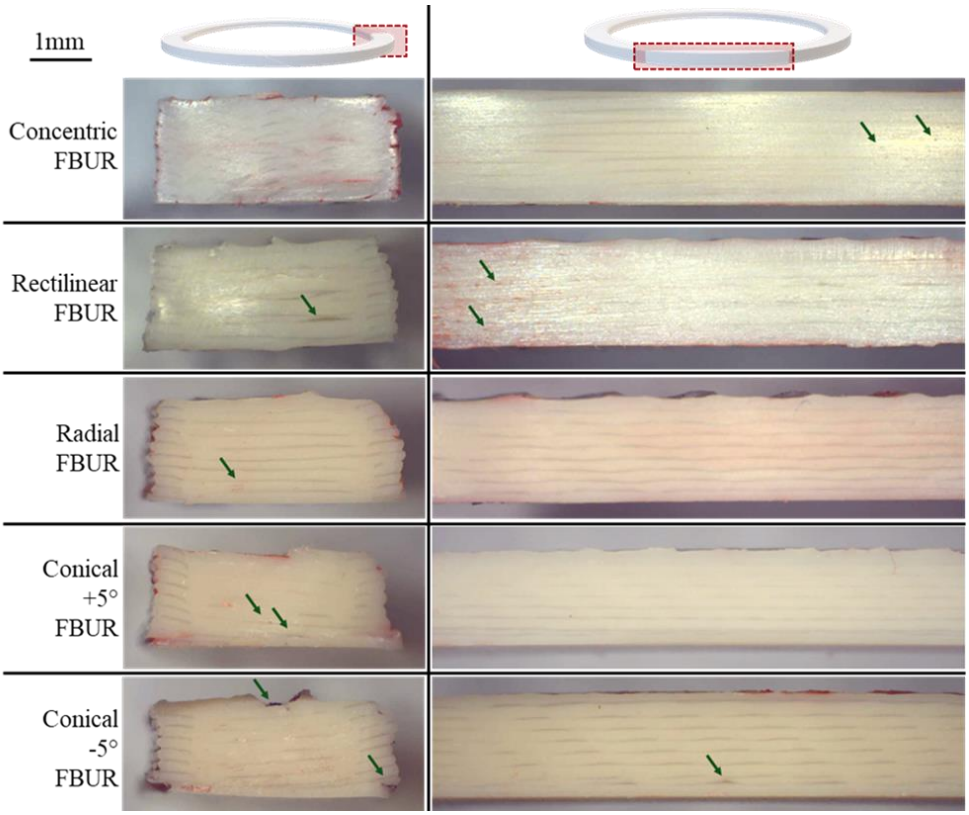

Figure 9 – Representative radial and circumferential cross sections of printed flat backup rings with different infill patterns. Red color which is visible on some of the cross sectioned surfaces is a dye which was used to penetrate voids to increase visibility. All infill patterns appear to be relatively low in void content. Green arrows highlight voids and deviations from the intended geometry. Specimen geometries closely match the desired shape of the flat backup ring. Bottom surface in these images corresponds with the build surface of the print bed and is the surface which is in contact with the O-ring in the sealing assembly.

Specific gravity and void content

The measured specific gravity and corresponding estimates of void volume fractions for each FBUR print pattern are presented in Table 2. The radial print pattern has the lowest void content and the rectilinear print pattern has the highest void content which are both consistent with the observations from optically analyzing FBUR cross sections.

Table 2- Specific gravity and void content

Print Pattern	Specific Gravity	Estimated Void Content (%)
Concentric	1.2879	2.43%
Rectilinear	1.2946	2.55%
Radial	1.318	0.15%
Conical +5°	1.2872	2.48%
Conical -5°	1.292	2.12%

Pressure vessel test results

The results presented in Figure 10 are the mean pressure vessel test results with the error bars set to one standard deviation in both directions. Images of the specimens after creep testing are presented in Figure 11. The mean and median results are presented in Table 3 including composite scores which are the extrusion to failure results divided by the corresponding creep results. Low creep deformation and high pressure at extrusion to failure are favorable indicators for sealing system performance. The worst mean performance for both tests is the concentric print pattern. The best performing print pattern for the extrusion to failure test is the conical +5° print pattern while the best performing print pattern for the creep tests is the rectilinear print pattern. The rectilinear print pattern resulted in the highest ranking as determined using the composite score which incorporates both metrics to indicate multi-objective performance. Note that an insufficient quantity of tests was performed to determine statistically significant differences between these results.

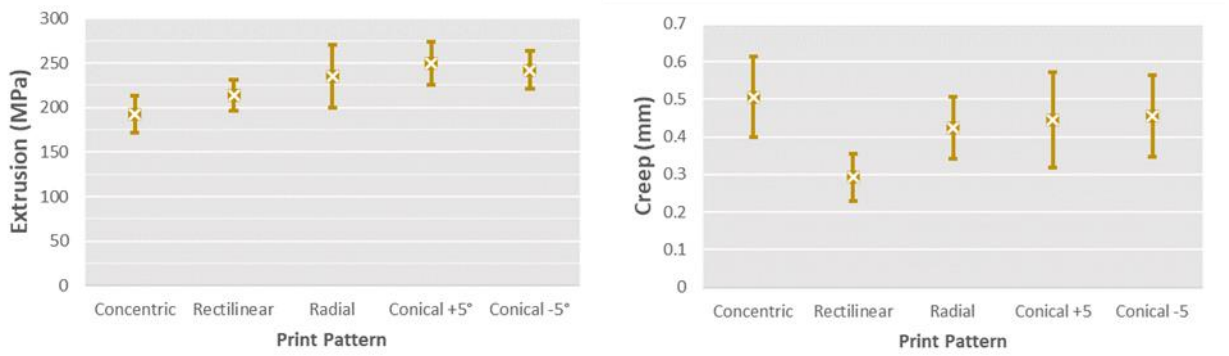

Figure 10 - Mean pressure vessel test results with error bars set to one standard deviation in each direction.

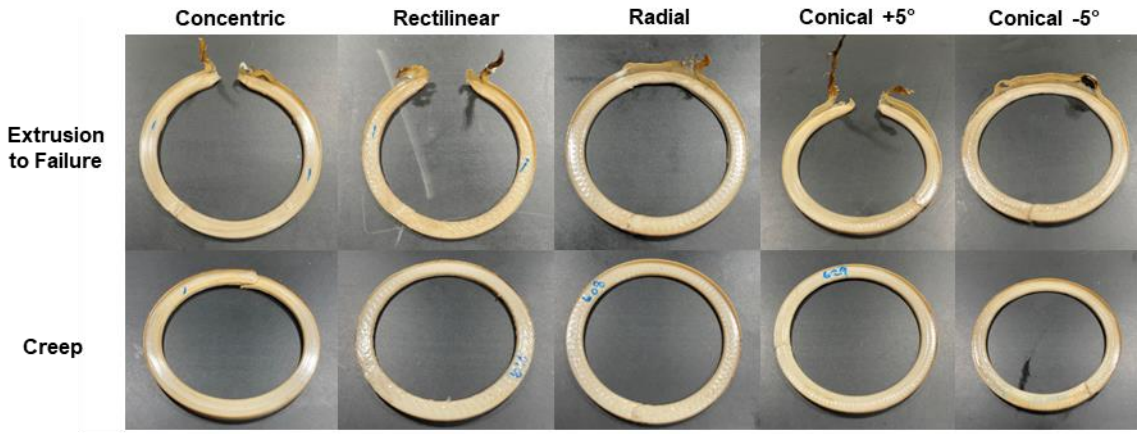

Figure 11 - Flat backup rings after pressure vessel testing. Each column corresponds with the print pattern. Each row corresponds with the test protocol.

Table 3 – Mean and median results from pressure vessel testing

	Extrusion (MPa)		Creep (mm)		Composite (Mpa/mm)	
Print Pattern	Median	Mean	Median	Mean	Median	Mean
Concentric	181	192	0.483	0.506	375	380
Rectilinear	217	214	0.273	0.292	796	732
Radial	219	235	0.451	0.423	485	554
Conical +5°	236	250	0.457	0.445	517	562
Conical -5°	237	242	0.476	0.455	498	532

Discussion

PEEK FBUR fabrication through thermoplastic AM may be advantageous due to its flexibility in producing a variety of geometries which may simplify the necessary supply chain. When using a conventional hotend and conventional print patterns, e.g. rectilinear FBURs, the specimens do not perform as well as their injection molded counterparts but may meet the minimum requirements for some applications and service conditions. Previous work demonstrated improvements in PEEK FBUR performance approaching the performance of their injection molded counterparts by varying the distribution of CF throughout the FBUR. This study advanced these techniques by developing a high-temperature mixing printer which supports the functions necessary for FVF control during PEEK FBUR fabrication. This printer was used in this work to evaluate advanced print patterns and compare them to conventional print patterns which characterizes the impact of print orientation on FBUR performance. The influence of print patterns on seal performance as compared to the influence of composite architectures is visualized by overlaying both sets of median results on the graph in Figure 12. Though these print patterns do not impact performance as much as the composite architectures do, these methods may be combined with the composite architectures to yield compounding benefits which may exceed the

performance of conventional FBURs. Future work should investigate such combinations of print patterns and composite architectures to further refine the design and corresponding print operations for increased performance without changes to the FBUR geometry. This work further informs future attempts to optimize for multi-objective performance. Toolpath selection when printing with an active mixing hotend may impact both the properties associated with print orientation and composition accuracy necessary for producing the desired composite architecture.

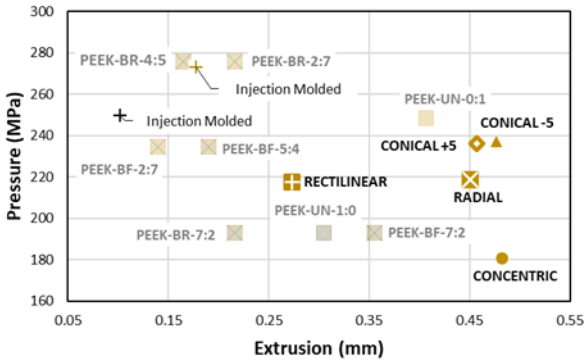

Figure 12 – Median pressure vessel tests plotted with creep results on the horizontal axis and pressure at rupture plotted on the vertical axis. Faded data points were extracted from the previous study and represent flat backup rings with a variety of composite architectures but have the same radial infill pattern [21].

The radial specimens printed in this study largely follow the same scheme for FBUR fabrication as the specimens from the previous study which are labelled "PEEK-UN-0:1." The previous radial PEEK FBUR (PEEK-UN-0:1) appears to have increased performance as compared to the Radial FBUR of this study. Two major differences exist between the two manufacturing processes used to produce these specimens. The newer specimens were manufactured using an active mixing hotend which causes rotational flow and therefore a different shear load and flow profile as the polymer is extruded. This is in contrast to the simpler shear and flow patterns experienced by the polymer when printing with a conventional hotend. Though this difference in hotend may impact the characteristics of the resulting FBUR, the more impactful difference in process parameters is likely the difference in the ambient temperature and the difference in bed temperature. The specimens in this study were printed in open air (approximately 24 °C) on a print bed which could only reach a maximum temperature of 160 °C. When produced in the previous study, the bed temperature was held at 200 °C and the ambient temperature was held at 70 °C. The crystallinity of PEEK has a significant impact on its properties and can be modified by heat treatment. Similarly, these differences in ambient conditions likely altered the crystallinity of the PEEK in favor of the specimen which was printed with elevated ambient and bed temperatures. Future work should investigate heat treatment procedures and enhanced environmental control systems within the printer.

The creep performance of the rectilinear specimen is surprising considering a relatively high proportion of voids were observed to be distributed near the perimeter, a region of the FBUR which experiences large loads due to proximity to the extrusion gap in the test vessel. The relatively low mean extrusion-to-failure results for the rectilinear specimen is consistent with the observations regarding quality of the rectilinear prints. This result regarding creep may partly be due to limitations of the measurement methodology to capture the deformation elsewhere in the

print such as near pores, e.g. measurement error of creep when densification is present within the creep test. Another possible explanation may be the alternating print pattern within the rectilinear FBURs which may favorably constrain deformation much like what is developed from different stacking sequences in fiber composite layups [23]. Future work should investigate more variation in the sequence of print patterns across layers to further enable tailoring for multi-objective performance.

Experimental studies like this one are time intensive and costly when compared to computational studies. Development of a computational model to predict seal performance would accelerate this research by enabling rapid investigations into a wide variety of designs and print configurations. Such a computational model with validation from experimental studies like this one are likely to yield significant advantages for AM sealing systems.

This study was also limited in its investigation into long-term seal performance when in service in a corrosive environment. Carbon capture and storage and applications in oil and gas are two examples of such applications which operate seals in a corrosive environment. Additively manufactured seals may contain interfaces and other features which accelerate corrosive effects. This too should be considered when designing AM FBURs. As an example, future AM FBUR designs may utilize LCC to keep CFs away from free surfaces where they may accelerate corrosive effects further increasing resistance to corrosion yielding another benefit to these techniques.

Conclusion

The observed relationship between test results and print orientation may inform tuning of sealing structures in numerous industries to further optimize seals for multiple objectives. The support for a simplified supply chain further highlights the value of this manufacturing methodology. With continued advancements and refinements to the composite architecture, print patterns, and base materials, AM FBURs will likely exceed the capabilities of their traditionally manufactured counterparts.

Acknowledgements

The authors wish to thank the students from UTEP for their help with this project, including Ramon Gamez, Baldomero Fuentes, and Daniel Hernandez for helping with the printer design and implementation. The authors wish to thank personnel at the Singapore Material Science Laboratory including Sandeep Thatathil and Li Huay Cheng for their support with testing. The authors wish to thank Halliburton management for permission to publish this work.

Funding

The authors wish to acknowledge the financial support provided by Halliburton Energy Services and the support from the UTEP Vice President of Student Affairs and Campus Office of Undergraduate Research Initiatives.

Conflict of Interest

The University of Texas System has a patent for technology described in this work for which Joshua T. Green is an inventor.

References

[1] M. Czepiel, M. Bańkosz, A. Sobczak-Kupiec, Advanced Injection Molding Methods: Review, Materials (Basel). 16 (2023). https://doi.org/10.3390/ma16175802.

[2] M. Lay, N.L.N. Thajudin, Z.A.A. Hamid, A. Rusli, M.K. Abdullah, R.K. Shuib, Comparison of physical and mechanical properties of PLA, ABS and nylon 6 fabricated using fused deposition modeling and injection molding, Compos. Part B Eng. 176 (2019) 107341. https://doi.org/10.1016/j.compositesb.2019.107341.

[3] A.R. Torrado, D.A. Roberson, Failure Analysis and Anisotropy Evaluation of 3D-Printed Tensile Test Specimens of Different Geometries and Print Raster Patterns, J. Fail. Anal. Prev. 16 (2016) 154–164. https://doi.org/10.1007/s11668-016-0067-4.

[4] G. Cicala, A. Latteri, B. Del Curto, A. Lo Russo, G. Recca, S. Farè, Engineering thermoplastics for additive manufacturing: A critical perspective with experimental evidence to support functional applications, J. Appl. Biomater. Funct. Mater. 15 (2017) e10–e18. https://doi.org/10.5301/jabfm.5000343.

[5] S.Z. Gebrehiwot, L. Espinosa-Leal, M. Andersson, H. Remes, On the Short-Term Creep and Recovery Behaviors of Injection Molded and Additive-Manufactured Tough Polylactic Acid Polymer, J. Mater. Eng. Perform. 32 (2023) 10412–10430. https://doi.org/10.1007/s11665-023-08278-6.

[6] K. Gong, H. Liu, C. Huang, Z. Cao, E. Fuenmayor, I. Major, Hybrid Manufacturing of Acrylonitrile Butadiene Styrene (ABS) via the Combination of Material Extrusion Additive Manufacturing and Injection Molding, Polymers (Basel). 14 (2022). https://doi.org/10.3390/polym14235093.

[7] A. Zhong, C. Glaesman, O-Ring Extrusions under High Pressure High Temperature Conditions, in: 198th Tech. Meet. Rubber Div. ACS, 2020. https://s3-prod.rubbernews.com/2021-10/RPN_20211018_tech_notebook.pdf.

[8] D. Kokkinis, F. Bouville, A.R. Studart, 3D Printing of Materials with Tunable Failure via Bioinspired Mechanical Gradients, Adv. Mater. 30 (2018) 1–9. https://doi.org/10.1002/adma.201705808.

[9] G.X. Gu, I. Su, S. Sharma, J.L. Voros, Z. Qin, M.J. Buehler, Three-dimensional-printing of bio-inspired composites, J. Biomech. Eng. 138 (2016) 1–16. https://doi.org/10.1115/1.4032423.

[10] I. Maskery, A. Hussey, A. Panesar, A. Aremu, C. Tuck, I. Ashcroft, R. Hague, An investigation into reinforced and functionally graded lattice structures, J. Cell. Plast. 53 (2017) 151–165. https://doi.org/10.1177/0021955X16639035.

[11] A. Panesar, I. Ashcroft, D. Brackett, R. Wildman, R. Hague, Design framework for multifunctional additive manufacturing: Coupled optimization strategy for structures with embedded functional systems, Addit. Manuf. 16 (2017) 98–106. https://doi.org/10.1016/j.addma.2017.05.009.

[12] B. Brenken, E. Barocio, A. Favaloro, V. Kunc, R.B. Pipes, Fused filament fabrication of fiber-reinforced polymers: A review, Addit. Manuf. 21 (2018) 1–16.

https://doi.org/10.1016/j.addma.2018.01.002.
[13] Y. Li, D. He, S. Yuan, K. Tang, J. Zhu, Vector field-based curved layer slicing and path planning for multi-axis printing, Robot. Comput. Integr. Manuf. 77 (2022). https://doi.org/10.1016/j.rcim.2022.102362.
[14] J. Plocher, A. Panesar, Review on design and structural optimisation in additive manufacturing: Towards next-generation lightweight structures, Mater. Des. 183 (2019). https://doi.org/10.1016/j.matdes.2019.108164.
[15] A. Panesar, I. Ashcroft, D. Brackett, R. Wildman, R. Hague, Design framework for multifunctional additive manufacturing: Coupled optimization strategy for structures with embedded functional systems, Addit. Manuf. 16 (2017) 98–106. https://doi.org/10.1016/j.addma.2017.05.009.
[16] Z.C. Kennedy, J.F. Christ, Printing polymer blends through in situ active mixing during fused filament fabrication, Addit. Manuf. 36 (2020) 101233. https://doi.org/10.1016/j.addma.2020.101233.
[17] H. Song, J. Martínez, P. Bedell, N. Vennin, S. Lefebvre, Colored fused filament fabrication, ACM Trans. Graph. 38 (2019) 1–11. https://doi.org/10.1145/3183793.
[18] W. Ye, H. Dou, J. Liu, Z. Li, Y. Cheng, D. Zhang, F. Yang, S. Jing, Additive manufacture of programmable multi-matrix continuous carbon fiber reinforced gradient composites, Addit. Manuf. 89 (2024) 104255. https://doi.org/10.1016/j.addma.2024.104255.
[19] T. Teng, Y. Zhi, M. Akbarzadeh, Single-Nozzle Multi-Filament System with Active Mixing for High-Fidelity Multimaterial Additive Manufacturing, Addit. Manuf. (2024). https://ssrn.com/abstract=4773564.
[20] J.T. Green, I.A. Rybak, J.J. Slager, M. Lopez, Z. Chanoi, C.M. Stewart, R. V. Gonzalez, Local composition control using an active-mixing hotend in fused filament fabrication, Addit. Manuf. Lett. 7 (2023). https://doi.org/10.1016/j.addlet.2023.100177.
[21] J.T. Green, I.A. Rybak, C. Glaesman, Backup-Ring Optimization for High-Temperature and High-Pressure Applications Through Dynamic Composition Modification in Composite 3d Printing, Int. Pet. Technol. Conf. IPTC 2024. (2024). https://doi.org/10.2523/IPTC-23353-MS.
[22] Home | Marlin Firmware, (2018). https://marlinfw.org/ (accessed July 25, 2023).
[23] M.S. Irfan, R.A. Alia, T. Khan, W.J. Cantwell, R. Umer, Time-temperature superposition of flexural creep response of carbon fiber PEKK composites manufactured using different prepreg stacking sequence, J. Thermoplast. Compos. Mater. 36 (2023) 1135–1153. https://doi.org/10.1177/08927057211051773.
PEEK The orientation of FVF architectures